

ARTICLE



Germline and sporadic mTOR pathway mutations in low-grade oncocytic tumor of the kidney

Payal Kapur^{1,2,3,8}, Ming Gao^{3,4,8}, Hua Zhong^{1,5,8}, Suneetha Chintalapati¹, Midori Mitui¹, Spencer D. Barnes⁵, Qinbo Zhou⁶, Jeffrey Miyata^{3,4}, Deyssy Carrillo^{3,4}, Venkat S. Malladi^{3,5}, Dinesh Rakheja^{1,3}, Ivan Pedrosa^{3,7}, Lin Xu⁶, Lisa Kinch⁶ and James Brugarolas^{3,4}

© The Author(s), under exclusive licence to United States & Canadian Academy of Pathology 2021

Low-grade oncocytic tumor (LOT) of the kidney is a recently described entity with poorly understood pathogenesis. Using next-generation sequencing (NGS) and complementary approaches, we provide insight into its biology. We describe 22 LOT corresponding to 7 patients presenting with a median age of 75 years (range 63–86 years) and male to female ratio 2:5. All 22 tumors demonstrated prototypical microscopic features. Tumors were well-circumscribed and solid. They were composed of sheets of tumor cells in compact nests. Tumor cells had eosinophilic cytoplasm, round to oval nuclei (without nuclear membrane irregularities), focal subtle perinuclear halos, and occasional binucleation. Sharply delineated edematous stromal islands were often observed. Tumor cells were positive for PAX8, negative for CD117, and exhibited diffuse and strong cytokeratin-7 expression. Six patients presented with pT1 tumors. At a median follow-up of 29 months, four patients were alive without recurrence (three patients had died from unrelated causes). All tumors were originally classified as chromophobe renal cell carcinoma, eosinophilic variant (chRCC-eo). While none of the patients presented with known syndromic features, one patient with multiple bilateral LOTs was subsequently found to have a likely pathogenic germline *TSC1* mutation. Somatic, likely activating, mutations in *MTOR* and *RHEB* were identified in all other evaluable LOTs. As assessed by phospho-S6 and phospho-4E-BP1, mTOR complex 1 (mTORC1) was activated across all cases but to different extent. *MTOR* mutant LOT exhibited lower levels of mTORC1 activation, possibly related to mTORC1 dimerization and the preservation of a wild-type *MTOR* copy (retained chromosome 1). Supporting its distinction from related entities, gene expression analyses showed that LOT clustered separately from classic chRCC, chRCC-eo, and RO. In summary, converging mTORC1 pathway mutations, mTORC1 complex activation, and a distinctive gene expression signature along with characteristic phenotypic features support LOT designation as a distinct entity with both syndromic and non-syndromic cases associated with an indolent course.

Modern Pathology (2022) 35:333–343; <https://doi.org/10.1038/s41379-021-00896-6>

INTRODUCTION

The differential diagnosis of renal tumors with exclusively eosinophilic (or oncocytic) cytoplasm traditionally involves differentiating a malignant tumor, chromophobe renal cell carcinoma (chRCC), in particular the eosinophilic variant (chRCC-eo), from benign renal oncocytoma (RO)^{1,2}. This distinction frequently poses a dilemma given their shared morphologic features especially with unifocal tumors in non-syndromic settings². Furthermore, markers often used in the differential diagnosis, such as cytokeratin (CK) 7 (typically diffuse in chRCC and rare scattered in RO), are not always able to distinguish chRCC-eo, which can have rare or patchy expressions. This difficulty is further compounded by a lack of definite criteria to distinguish chRCC-eo from the classic variant of chRCC.

The differential diagnosis of renal tumors with eosinophilic cytoplasm has become even more challenging with newly

described entities^{2,3}. These include tuberous sclerosis complex (TSC)- associated renal cell carcinoma (RCC)^{4,5}, hybrid oncocytic/ chromophobe tumors (HOCT) in the setting of Birt-Hogg-Dubé (BHD) syndrome⁶, eosinophilic solid and cystic RCC (ESC RCC)^{7–9}, MiT family translocation RCC^{10,11}, succinate dehydrogenase (SDH)-deficient RCC¹², fumarate hydratase (FH)-deficient RCC¹³, eosinophilic vacuolated tumors (EVT)/ RCC with eosinophilic and vacuolated cytoplasm^{14–17}, as well as other currently unclassified RCCs¹⁸.

Recently, a distinct low-grade oncocytic tumor (LOT) was reported as a potential new entity^{19,20}. Two publications describe LOT as unifocal small tumors (mean size 3.9 cm [range 1.1–13.5 cm]), devoid of aggressive features in non-syndromic settings^{19,21}. Histologically, LOT has a predominantly solid architecture composed of tight nests with foci of delineated edematous

¹Department of Pathology, University of Texas Southwestern Medical Center, Dallas, TX, USA. ²Department of Urology, University of Texas Southwestern Medical Center, Dallas, TX, USA. ³Kidney Cancer Program at Simmons Comprehensive Cancer Center, University of Texas Southwestern Medical Center, Dallas, TX, USA. ⁴Department of Hematology-Oncology Division of Internal Medicine, University of Texas Southwestern Medical Center, Dallas, TX, USA. ⁵Lyda Hill Department of Bioinformatics, University of Texas Southwestern Medical Center, Dallas, TX, USA. ⁶Department of Population and Data Sciences, University of Texas Southwestern Medical Center, Dallas, TX, USA. ⁷Department of Radiology, University of Texas Southwestern Medical Center, Dallas, TX, USA. ⁸These authors contributed equally: Payal Kapur, Ming Gao, Hua Zhong. [✉]email: payal.kapur@utsouthwestern.edu; james.brugarolas@utsouthwestern.edu

Received: 15 March 2021 Revised: 3 August 2021 Accepted: 4 August 2021

Published online: 20 September 2021

stroma that contains strands of tumor cells. The tumor cells have eosinophilic/oncocyctic cytoplasm, uniform round nuclei without significant irregularities, and only focal subtle perinuclear halos. They have a characteristic but unexpected immune profile: they are CD117 (c-kit) negative and show strong and diffuse CK7 reactivity. To date, all tumors have been reported to be associated with an indolent clinical course^{2,19,20,22}.

We previously published a comprehensive genomic analysis of 167 primary non-clear cell RCC that included RO ($n = 31$), renal oncocyctic neoplasm (RON) ($n = 5$), and chrRCC (36 classic variants; 12 eosinophilic variants)²³. Notably, the majority of chrRCC-eo lacked characteristic DNA copy number alterations of the classic variant of chrRCC. Two of the 12 chrRCC-eo morphologically fit the description of LOT^{19,20,24} and were CD117 negative/CK7 positive. Interestingly, both tumors had a unique gene expression signature and harbored mammalian target of rapamycin (*MTOR*) mutations. These results led us to hypothesize that LOT may be characterized by a unique gene expression signature and mutations of the mammalian target of rapamycin complex 1 (mTORC1) pathway (such as in *MTOR*, *TSC1*, *TSC2*, or *RHEB*). In the current study, we evaluate this notion through systematic analyses of eosinophilic tumors at our institution that fit the morphology and immunohistochemistry profiles of LOT.

MATERIALS AND METHODS

Case selection

The study was conducted with approval by the UT Southwestern Medical Center (UTSW) Institutional Review Board (IRB) and according to the Health Insurance Portability and Accountability Act (HIPAA) guidelines. We searched our institutional RCC database (Kidney Cancer Explorer [KCE]; sponsored by the UT Southwestern [UTSW] Kidney Cancer NIH SPORE grant, the Lyda Hill Department of Bioinformatics, and the Bioinformatics Core Facility) for tumors diagnosed as chrRCC, RON, and RO. We excluded diagnoses based on biopsy specimens as well as consultation cases. Between 2005 and 2016, 204 cases (99 chrRCC, 20 RON, and 85 RO) were identified out of a total of 1870 renal tumors, including some that were published previously²³. Archival material, where available, was retrieved (204 cases) and re-reviewed by two genitourinary (GU) pathologists (S.C. and P.K.), who classified these tumors as LOT based on previously described characteristic morphology and IHC (CK7 diffuse+/CD117-)¹⁹. Additional IHCs were obtained as needed during review (CK7 and CD117, CK20, cathepsin K, TFEB [transcription factor EB], TFE3 [transcription factor E3], SDHB [succinate-dehydrogenase B], and FH [fumarate hydratase]).

Clinical data

Patient age at nephrectomy, race, sex, tumor size, AJCC TNM staging categories, histologic subtype, date of surgery, date of development of metastases, and date of the last follow-up were collected from KCE. The tumors were staged based on the 2018 American Joint Committee on Cancer (AJCC) TNM classification for pathologic staging. Data in KCE were complemented through a comprehensive review of clinical data and pathology slides.

Immunohistochemistry

IHC analysis was performed on representative 3–5 μ m formalin-fixed paraffin-embedded (FFPE) whole tumor tissue sections. Staining for routinely used markers including Pax8 (10336-1-A P, 1:1000; Proteintech), carbonic anhydrase-IX/9 (CA9) (11071-1-AP, 1:100; Thermo Fisher), CD10 (56C6, 1:40; Dako), CK7 (M7018- OV-TL 12/30, 1:100; Dako), CK20 (7019-Ks20.8, 1:50; Dako), CD117 (A4502, 1:700; Dako), Melan A (7196-A103, 1:200; Dako), cathepsin-K (37259-3F9, 1:100; Abcam), FH (100743-J13, 1:1500; Santa Cruz), SDHB (14714-21A11, 1:100; Abcam), TFE3 (MRQ-37, 1:200; Cell Marque), TFEB (166736, 1:100; Santa Cruz), vimentin (M0725, 1:75; Dako), phospho-S6 (Ser240/244) (p-S6) (5364-D68F8, 1:300; Cell Signaling Technology) and phospho-4E-BP1 (Thr37/46) (p-4EBP1) (236B4, 1:800; Cell Signaling Technology) was performed using a Dako automated system (Agilent).

Immunoreactivity was interpreted as “negative” if <5% tumor cells stained positively. P-S6 and p-4EBP1 expression were determined based on

the percentage of tumor cells staining positive and the intensity of expression.

Next-generation sequencing

All hematoxylin and eosin (H&E) FFPE slides were examined to select the most representative areas from 7 LOTs as well as matched normal tissues. Corresponding areas were macrodissected (LOT 3–7). The tissue was submitted to BGI Genomics for DNA extraction and whole-exome sequencing (WES). DNA libraries were sequenced to an average read depth >100 \times for exome sequencing using 2 \times 75-base paired-end on a HiSeq2500 platform (Illumina, San Diego, CA, USA). DNA from LOT 7 tumor and LOT 6 normal did not pass quality control. The two index cases (LOT 1–2) were previously evaluated using fresh frozen tissue with simultaneous extraction of both DNA and RNA to enable integrative genomic analyses²⁵ and sequencing was performed as described previously²³.

Sanger sequencing

Validation of the *MTOR*, *TSC1*, *RHEB* mutations was carried out using PCR followed by Sanger sequencing on an ABI 3700. In total, 20 ng of patient DNA from normal and tumor samples was amplified using primers designed to capture each of the mutations in LOT 3–6. Normal tissue from LOT 6 had not passed quality control and more tissue was not available for further analysis. Oligonucleotide primer sequences are available on request.

Molecular analysis

Exome-seq reads from FASTQ files were aligned to the human reference genome GRCh38 (hg38) using the Burrows-Wheeler Aligner algorithm (BWA-MEM; version 0.7.17) set to default parameters²⁶. BAM files were generated using Picard Tools (version 2.20.5) to add read group information and sambamba was used to mark PCR duplicates. GATK toolkit (version 4.0.7)^{27–29} was used to perform base quality score recalibration and local realignment around indels. MuTect2³⁰, VarScan (v2.4.0)³¹, Shimmer (v0.2)³², SpeedSeq (v0.1.2)³³, Manta (v1.6.0), and Strelka2 (v2.9.10)³⁴ were used to call somatic variants and small-scale insertions and deletions (indels) for each tumor. A mutation that was repeatedly called by any two of these software tools was retained. Anovar was used to annotate germline/somatic mutations and indels³⁵. A minimum of 7 total reads in the normal sample and at least 3 variant reads in the tumor sample with a variant allele frequency (VAF) \geq 5% were required for somatic mutation calling. Intronic, untranslated region and intergenic mutations outside splice sites were filtered out. Missense mutations predicted to be benign by both PolyPhen-2 and SIFT (with <5% chance of inducing functional changes at the protein level) were filtered out³⁶. Somatic variant calls were inspected using Integrated Genomics Viewer v2.3.4 (IGV; Broad Institute, MIT Harvard, Cambridge, MA, USA). Variants were classified according to the American College of Medical Genetics and Genomics (ACMG) 2015 Guidelines. COSMIC and ClinVar were used as additional databases to annotate cancer relevance and clinical potential for detected variants.

We carried out somatic copy number variation (CNV) analyses on our exome-seq data using CNVkit with default parameters on tumor-normal pairs. CNVkit uses both on- and off-target sequencing reads to calculate log₂ copy ratios across the genome for each sample and improves accuracy in copy number calling by applying a series of corrections³⁷. Arm gain or loss was called when >50% of the chromosome exhibited copy number gain or loss³⁸.

RNA-seq reads were aligned to the human reference genome GRCh38 (hg38) using STAR³⁹ with the parameters “-runThreadN 48 -outSAMtype BAM Unsorted -outReadsUnmapped Fastx.” The FeatureCounts⁴⁰ software program with parameters “-primary -O -t exon -g transcript_id -s 0 -T 48 -largestOverlap -minOverlap 3 -ignoreDup -p -P -B -C” was used to measure gene expression levels. The human genome annotation file employed by FeatureCounts was downloaded from the UCSC table browser under the RefSeq Gene track. Genes were kept if they had at least 10 read counts in one or more of the 141 samples evaluated (2 LOT, 35 RO [including 4 RON-favor RO], 9 chrRCC-eo [including 1 RON-favor chrRCC-eo], 35 classic chrRCC, and 60 normal kidneys). These data were integrated with 89 TCGA cases (4 LOT, 15 chrRCC-eo, 46 classic chrRCC, and 24 normal kidney samples) for downstream analyses. Two tumor/normal RO pairs believed to have tumor/normal labels transposed were removed from the gene expression analyses: sample 13730 N, which was labeled as a normal and had a non-coding mutation [m.564:G>A] previously reported to occur in RO⁴¹ and its corresponding tumor (13730 T), which lacked the mutation;

and sample XP174N, which had a frameshift insertion [m.11866:A>AC] on *MT-ND4* also reported in RO⁴¹ and its corresponding tumor (XP174T), which lacked the mutation. The Bioconductor packages edgeR⁴² (version 3.28.1) and sva (version 3.34.0) were employed to perform normalization (using TMM⁴³) and batch effect removal (using ComBat⁴⁴). EdgeR was further utilized to: (1) identify differentially expressed genes (DEGs) between LOT and chRCC-*eo* types, and (2) perform KEGG analysis of DEGs to identify significantly enriched pathways with *p*-values ≤ 0.05.

RESULTS

Study cohort

From among 204 cases between 2005 and 2016 of chRCC, RON, and RO at our institution with adequate material, we identified 22 tumors corresponding to 8 nephrectomy/partial nephrectomy cases and seven patients that fit the morphologic description of LOT. Overall, LOT represented 4% (8 of 204 cases) of reviewed cases and 0.4% of all nephrectomies for renal tumors at our institution during the study timeframe. All 22 tumors had been originally diagnosed as chRCC-*eo*.

Baseline Clinical Characteristics And Clinical Course

The patient demographics and tumor characteristics are summarized in Table 1. The patients ranged from 63 to 86 years at diagnosis (mean age: 75 years). There were more females than males (M:F ratio, 2:5). None of the patients had a prior documented history of a syndrome including TSC and BHD. Suspicious skin lesions, pneumothoraxes, unexplained seizures, angiomyolipomas, or other characteristic syndromic features were not documented. Three patients, however, had multiple renal masses. One patient (LOT 3) had multiple bilateral renal tumors (6 on the right and 10 on the left) (Supplementary Fig. 1A, B). The patient was found to have a likely pathogenic germline variant in the *TSC1* gene. The patient received therapy with a mTORC1 inhibitor, everolimus, which led to remission of several lesions and stabilization of the rest. Another patient (LOT 5) had a history of prior nephrectomy for a benign renal tumor at an outside institution, and another (LOT 7) was found to have a concurrent contralateral second renal mass. Neither LOT 5, nor LOT 7, were found to have a genetic predisposition. Amongst the solitary LOTs, there was a predilection for the right kidney (right: 5; left: 1). Most patients underwent partial nephrectomy. At the time of this analysis, three patients were deceased due to unrelated causes including LOT 1, who expired from a subsequently diagnosed contralateral metastatic clear cell RCC. The 4 remaining patients were alive with no evidence of metastatic disease at the time of the last follow-up. Follow-up ranged from 3 months to 53 months (median 29 months).

Imaging features

Computed tomography (CT) was available in four patients (LOT 1–4). All masses exhibited areas with intense enhancement (i.e., similar to that of renal cortex) during the corticomedullary phase likely signifying pronounced angiogenesis (Supplementary Fig. 1). LOT 3 had multiple bilateral renal masses with similar appearance (Supplementary Fig. 1A, B). These tumors also demonstrated irregular areas of decreased central enhancement with some degree of progressive centripetal enhancement during the excretory phase (Supplementary Fig. 1B). Renal imaging confirmed the absence of classic angiomyolipoma features (i.e., macroscopic fat) in all cases evaluated.

Pathologic features

Grossly, the tumors were noted to be well-circumscribed, solid, tan to brown, and homogenous on the cut surface. Tumors ranged from 0.5 to 7.8 cm in size (mean: 3.1 cm). Areas with loose myxoid stroma, similar to oncocytomas, were appreciated grossly. None of

Table 1. Clinicopathologic Characteristics of LOTs in the Cohort.

Patient ID	Age	Sex	Presentation	Family History	Other Significant Medical History	Original Diagnosis	Nephrectomy	Laterality	Tumor Size (cm)	Focality (number)	pT	pN	Stage	Metastasis	Follow-up (months)
LOT 1	79	F	Back pain	None	Contralateral metastatic ccRCC	ChRCC- <i>eo</i>	Partial	Right	7.8	Unifocal	pT2a	pNx	II	No	Deceased (26)
LOT 2	86	F	Incidental	None	None	ChRCC- <i>eo</i>	Radical	Right	6.5	Unifocal	pT1b	pNx	I	No	ALF (3)
LOT 3a	63	F	Anemia	Father with b/l NX for unknown reason	B/l multiple LOTs	ChRCC- <i>eo</i>	Partial	Right	4.0, 2.3, 1.5, 1.4, 0.8, 0.5	Multifocal (6)	pT1a ^a	pNx	I	No	ALF (37)
LOT 3b						ChRCC- <i>eo</i>	Partial	Left	5.3, 5.2, 4.9, 3.7, 2.1, 2.0, 1.9, 1.6, 1.0, 0.9	Multifocal (10)	pT1b ^a	pNx	I	No	
LOT 4	69	M	Hematuria	None	None	ChRCC- <i>eo</i>	Partial	Right	2.3	Unifocal	pT1a	pNx	I	No	ALF (29)
LOT 5	71	F	Incidental	None	Prior contralateral nephrectomy for benign tumor	ChRCC- <i>eo</i>	Partial	Right	3.8	Unifocal	pT1a	pNx	I	No	ALF (53)
LOT 6	75	F	Incidental	None	None	ChRCC- <i>eo</i>	Partial	Left	2.4	Unifocal	pT1a	pNx	I	No	Deceased (36)
LOT 7	84	M	Incidental	None	Contralateral renal mass followed with AS	ChRCC- <i>eo</i>	Radical	Right	6.5	Unifocal	pT1b	pNx	I	No	Deceased (29)

ccRCC clear cell renal cell carcinoma, b/l bilateral, NX nephrectomy, AS active surveillance, ChRCC-*eo* chromophobe renal cell carcinoma, eosinophilic variant, ALF alive at last follow-up. ^apT represents the highest stage.

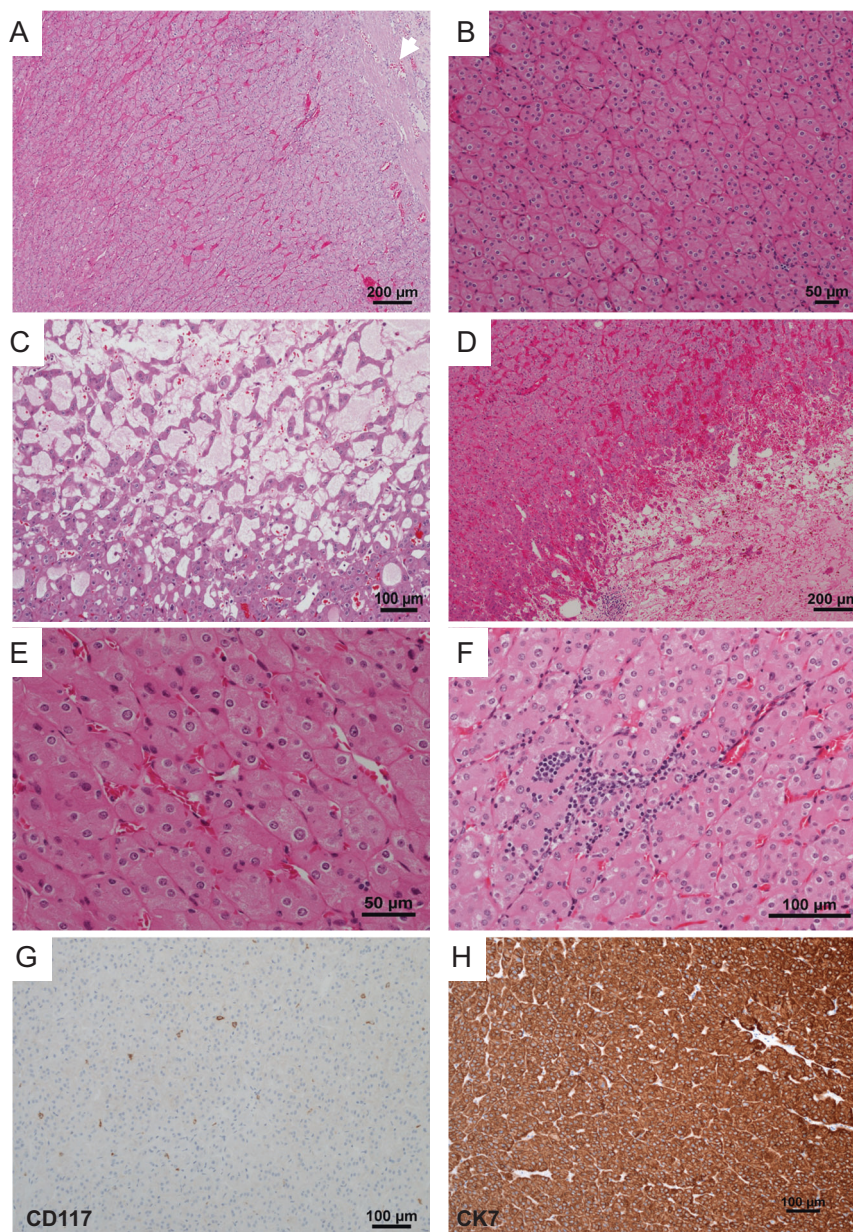


Fig. 1 Histologic characteristics of LOT. Representative H&E images from LOT reveal a well-circumscribed partly encapsulated eosinophilic tumor (white arrow) (A) composed of homogenous cells arranged in sheets of tight nests (B) with focal edematous areas with loose cords of tumor cells (C), and occasional dilated vascular channels and hemorrhage (D). High-power images show that the tumors are uniformly composed of cells with abundant finely granular eosinophilic cytoplasm, indistinct cell borders, round nuclei with relatively smooth membranes, subtle perinuclear clearing, and binucleation (E). Lymphoid clusters are frequent (F). Representative immunohistochemical profile of CD117 with only scattered positive mast cells (G), and cytokeratin 7, which is strong and diffusely positive (H).

the tumors had renal sinus involvement (Table 1). AJCC pathologic T stage was pT1a in 4/8, pT1b in 3/8, and pT2a in 1/8.

A review of the H&E slides demonstrated striking morphologic similarities in all 22 tumors. All tumors were well-demarcated, either devoid of or with a thin partial peripheral fibrous pseudocapsule (Fig. 1A). At low power, tumors were homogenous and solid. They were composed of sheets of compact uniform small nests (Fig. 1A, B). Abrupt areas of hypocellular, loose edematous stroma with scattered cords of tumor cells were present (Fig. 1C). In some tumors, focal areas of hemorrhage and dilated vascular channels filled with serous or hemorrhagic fluid were also seen (Fig. 1D). The tumor cells were uniform, polygonal in shape, and had ill-defined cell borders (Fig. 1E). They contained eosinophilic, finely granular, cytoplasm, and central round to

mildly oval nuclei with focal mild nuclear membrane irregularities and prominent small eosinophilic nucleoli (Fig. 1E, F). Subtle perinuclear clearing, mild pleomorphism, and binucleation were seen in all cases, more apparent focally in some cases. Focal scattered small clusters of lymphocytes and histocytes were also seen (generally near the loose stromal areas) (Fig. 1F). Tumor necrosis, frequent or atypical mitosis, nuclear pleomorphism, cytoplasmic clearing, cytoplasmic stippling, or inclusions were not identified. Typical features of classic chRCC (wrinkled, raisinoid, nuclear membrane; marked perinuclear clearing; well-defined cell borders; clear cytoplasm) were not apparent. Peritumoral blood vessels were markedly thick-walled in the majority of cases (Supplementary Fig. 2A). All 16 tumors in the patient with the germline *TSC1* mutation (LOT 3) showed similar features with the

Table 2. Immunohistochemical Profile of LOTs in the Cohort.

Patient ID	CD117	CK7	P-S6		P-4EBP1	
			Intensity	Percentage	Intensity	Percentage
LOT 1	Negative	Diffuse strong positive	Moderate	20	Weak-moderate	30
LOT 2	Negative	Diffuse strong positive	Weak-moderate	5	Weak-moderate	5
LOT 3a ^a	Negative	Diffuse strong positive	Moderate-strong	90	Weak-moderate	40
LOT 3b ^a	Negative	Diffuse strong positive	Strong	90	Moderate	60
LOT 4	Negative	Diffuse strong positive	Strong	75	Moderate	50
LOT 5	Negative	Diffuse strong positive	Moderate	80	Moderate	50
LOT 6	Negative	Diffuse strong positive	Moderate	30	Weak-moderate	20
LOT 7	Negative	Diffuse strong positive	Weak-moderate	5	Weak	5

^aRepresentative section from a total of 5 tumors was evaluated by immunohistochemistry.

addition of small tumorlets in the adjacent renal parenchyma (Supplementary Fig. 2B). Consistent with the imaging findings, no angiomyolipomas were identified in adjacent kidney sections. A small distinct area (3.0 mm) with slightly different morphology was observed in one of the 16 tumors with large intracytoplasmic vacuoles similar to EVT (Supplementary Fig. 2C, D). A small distinctive area (4.0 mm) was also seen in a LOT 4 tumor with more pronounced perinuclear clearing and nuclear membrane irregularities (Supplementary Fig. 2E, F).

Immunohistochemical features

LOTs (including representative sections from multiple tumors in LOT 3) were interrogated with immunohistochemical (IHC) stains. All LOTs showed diffuse and strongly reactive cytokeratin 7 and were negative for CD117 (Table 2, Fig. 1G, H). They were positive for PAX8, retained FH as well as SDHB, and were negative for TFE3 and TFEB. They were also negative for HMB45/Melan A, cytokeratin 20, cathepsin K, and CA9. Whenever performed, E-cadherin was positive whereas CD10 and vimentin were negative.

Molecular features

Whole exome sequencing (WES) was available for 2 cases (LOT 1, 2) from our previously published study²³. Among the new cases (LOT 3–7), DNA from the tumor region of LOT 7 and the normal kidney of LOT 6 did not pass quality control. WES from 5 tumors with paired normal samples demonstrated mutations in mTORC1 pathway genes (*MTOR*, *TSC1*, or *RHEB*) in all cases (Table 3, Supplementary Fig. 3). In addition, unpaired WES analyses from the LOT 6 tumor also showed an *MTOR* gene mutation (Table 3, Supplementary Figs. 4A and 5). Variant calls were inspected using the Integrated Genomics Viewer (IGV; Supplementary Fig. 4). Mutations were validated by Sanger sequencing on available tumor and normal samples (Supplementary Fig. 5).

The presence of mTORC1 pathway gene mutations across all the samples (LOT 1, 2, 5, 6 [*MTOR*], LOT 3 [*TSC1*], and LOT 4 [*RHEB*]) (Table 3) suggested that mTORC1 may play a role in LOT development. To evaluate this notion further, we assessed the particular mutations. While *RHEB* and mTOR are positive regulators of mTORC1 and mutations would be expected to be activating, *TSC1* is a negative regulator and mutations would be expected to inactivate it. A likely pathogenic germline *TSC1* variant was detected in the blood (and normal kidney sample) from LOT 3. The mutation caused a substitution of two nucleotides after exon 15 of the *TSC1* gene (NM_000368.4:c.2208 + 2 T > A) and was predicted to abolish the native splice donor site (Supplementary Fig. 4B). In addition, a somatic frameshift *TSC1* mutation (p.Arg760Serfs*2) was found in the tumor (Table 3, Supplementary Fig. 4A). mTOR mutations were found in LOT 1 (mTOR p.L2427Q), LOT 2 (mTOR p.S2215Y), LOT 5 (mTOR p.S2413L) and LOT 6 (mTOR

p.K1452_E1455del). Consistent with their being activating, 3 out of the 4 mTOR mutations affected a residue previously shown to be mutated in other tumors (<https://www.cbioportal.org>; <https://cancer.sanger.ac.uk/cosmic>)^{45,46}. Furthermore, two mutations (p.L2427Q and p.S2215Y) were previously shown to activate mTORC1 in studies in vitro^{45–47}. A mutation in *RHEB* in LOT 4 (*RHEB* p.Y35L) was both previously reported in other tumors (<https://www.cbioportal.org>) and shown to be activating in vitro⁴⁵.

To evaluate the functional significance of the least characterized mTOR mutations (K1452-E1455 deletion and p.S2413L), we assessed their impact on the mTORC1 structure. We mapped the mutations onto the crystal structures of both the apo and *RHEB*-activated mTOR proteins (Fig. 2A). Previously published cancer-associated mTOR mutations leading to kinase hyperactivation tend to occur at specific areas including the FAT hinge (i.e., A1459P) and the interface between the kinase C-lobe and FAT domain (i.e., E2419K) where they destabilize the apo state^{48–50}. The K1452-E1455 deletion removes a single turn from a hinge helix in the FAT domain near the known hyper-activating A1459 mutation (Fig. 2B left). The turn interacts with neighboring helices that adopt alternate conformations in the inactive and active states and the deletion would remove helical interactions from both states suggesting increased flexibility at the hinge that could lead to hyperactivation. The mTOR p.S2413L mutation resides in the kinase C-lobe at the FAT domain interface. This interface also adopts alternate conformations in the active and inactive states (Fig. 2B right). Another known activating mutation (E2419K) is found in the same C-lobe helix at the FAT interface and is thought to lower the barrier to activation^{48,50}. Overall, these data are consistent with the notion that the K1452-E1455 deletion and p.S2413L substitution are similarly activating as other previously reported mTOR mutations tested in vitro.

To evaluate the impact of these mutations on mTORC1 activity, we analyzed p-S6 (Ser240/244) and p-4EBP1 (Thr37/46). All LOTs evaluated showed p-S6 expression in at least 5% tumor cells (Fig. 3). Similar results were observed for p-4EBP1 (Fig. 3).

However, we observed a range of mTORC1 activation. Higher activation was observed in LOT 3, 4, and 5, but LOT 1, 2, 6, and 7 had lower levels (Fig. 3). These data suggested a correlation between *MTOR* mutation (LOT 1, 2, 5, 6) and lower mTORC1 activity (LOT 1, 2, 6, and 7). Specifically, 3/4 cases with *MTOR* mutations had lower levels of mTORC1 activation (LOT 1, 2, 6). One potential explanation for the moderate p-S6 and p-4EBP1 activation levels in these cases may be the presence of a wild-type *MTOR* allele and protein, in particular since mTORC1 dimerizes. NGS and Sanger studies were consistent with the presence of a wild-type *MTOR* allele suggesting that mutations were heterozygous. Furthermore, copy number analyses available for 3 out of the 4 cases (a normal sample is missing for LOT 6) showed two copies of chromosome 1, where *MTOR* is located

Table 3. Molecular Alterations identified in LOTs in the Cohort.

Patient ID	Genomic ID	Chromosome	Start position	End position	Reference sequence	Tumor sequence	Matched normal sequence	Gene	Variation classification	Validation method	Somatic mutation ^a	Amino acid alteration
LOT 1	XP238T	chr1	11114338	11114338	A	T	A	MTOR	Nonsynonymous SNV	Prior	NM_004958.3:c.7280T>A	p.Leu2427Gln
LOT 2	17827T	chr1	11124516	11124516	G	T	G	MTOR	Nonsynonymous SNV	Prior	NM_004958.3:c.6644C>A	p.Ser2215Tyr
LOT 3a	KC02816-T1-FFPE	chr9	132902719	132902719	A	AGCTT	A	TSC1	Frameshift substitution	Sanger	NM_000368.4:c.2273_2276dup	p.Arg760Serfs*2
LOT 4	KC02129-T1-FFPE	chr7	151490963	151490964	TA	AG	TA	RHEB	Nonsynonymous SNV	Sanger	NM_005614.3:c.103_104delinsCT	p.Tyr35Leu
LOT 5	KC02942-T2-FFPE	chr1	11114380	11114381	CT	AG	CT	MTOR	Nonsynonymous SNV	Sanger	NM_004958.3:c.7237_7238delinsCT	p.Ser2413Leu
LOT 6	KC00627-T1-FFPE	chr1	11157255	11157267	ACTCTGTCAGTTT	A	Not available	MTOR	Nonframeshift substitution	Sanger	NM_004958.3:c.4354_4365del	p.Lys1452_Glu1455del
LOT 7	Not pass the quality check					Not available	Not available					

^aSomatic mutation was confirmed by Sanger.

(1p36.22) (Supplementary Fig. 6). mTOR forms a dimer with two interfaces between N-heat and M-heat domains. In the apo structure, the N-heat domain is positioned in a relatively open state with respect to the rest of the protein (Fig. 2C left). Upon RHEB binding, the N-heat domain rotates toward the intersection of the M-heat and FAT domains, and the kinase catalytic cleft closes to align active site residues for catalysis^{48,51}. This rotation approximates the dimer interaction surfaces (Fig. 2C right). The changes induced by RHEB binding are not compatible with a mixed dimer of activated and inactivated mTOR⁴⁸. Furthermore, RHEB-induced kinase activation is cooperative in the wild-type complex⁴⁸. In the absence of RHEB, mTOR could adopt a heterogeneous mixture of activation states depending upon whether it is constituted by wild-type dimers, heterodimers (of wild-type and mutant), or mutant dimers. Thus, the presence of a wild-type subunit could potentially reduce the impact of hyperactivating mTOR mutations. The overall mTORC1 activation state as compared, for instance, to tumors in which mTORC1 activation is driven by a single mutant protein (with loss of the wild-type allele) or by activation upstream (such as through *RHEB* or *TSC1/TSC2* mutations) may be reduced.

To extend the findings in our cohort, we reviewed all tumors categorized as chRCC-*eo* in the TCGA (KICH) project⁵². We used the NIH GDC Data Portal to review digital slides (www.portal.gdc.cancer.gov). While IHCs are unavailable (CK7+/CD117– status could not be confirmed), 4 out of 19 tumors morphologically resembled LOT (TCGA-KN-8437, TCGA-KM-8439, TCGA-KM-8441, TCGA-KM-8639). We assessed the mutation status of mTORC1 pathway genes in these 4 tumors. Interestingly, 2 of these tumors had pathogenic mTOR mutations (TCGA-KN-8437; p.L2427R and TCGA-KM-8441; p.I2017T) (Supplementary Fig. 7A, B). TCGA-KN-8437 had a mutation in the same residue as LOT 1 in our cohort and the particular substitution, L2427R, has been shown to be a gain of function mutation in the literature¹⁸. Similarly, the mTOR mutation in TCGA-KM-8441 (p.I2017T) has been previously reported in tumors and shown to induce kinase activity *in vitro*⁵³. Both tumors were reported to be diploid and without chromosome 1 loss. A third TCGA tumor had a pathogenic frameshift *TSC1* mutation (TCGA-KM-8639; p.R718Pfs*3). No mutations were found in mTORC1 pathway genes in the fourth tumor.

Consistently, all LOTs cases in our cohort were diploid with all 22 autosome pairs (Fig. 4). None of the cases showed iconic chromosomal alterations of other RCCs, such as multiple chromosomal losses, which typify chromophobe RCC, 3p loss in clear cell RCC, or gain of chromosome 7 and 17 as seen in papillary RCC.

We next asked how LOTs relate to other RCCs and performed gene expression analyses. Whole transcriptome data was available for six cases (LOT 1–2 from UTSW²³ and the 4 TCGA LOTs⁵²). We compared the gene expression profiles with those from chRCC-*eo* (9 from UTSW including 1 RON-favor chRCC-*eo*²³ and 15 from TCGA⁵²), classic chRCC (35 from UTSW²³ and 46 from TCGA⁵²), and RO (33 from UTSW including 4 RON-favor RO²³). In addition, normal kidney samples (60 from UTSW²³ and 24 from TCGA⁵²) were included. We generated a t-distributed stochastic neighbor embedding (t-SNE) plot, which showed tight clustering of the LOT cases, away from RO, chRCC-*eo*, classic chRCC, and normal kidney (Fig. 5A). Intriguingly, LOT clustered away even from chRCC with mTORC1 pathway gene mutations (Fig. 5A).

We then focused on chRCC-*eo* and LOT due to their morphological similarity. We found 1674 DEGs between LOT and chRCC-*eo* tumor samples at a false discovery rate (FDR) ≤ 0.05 with an absolute log₂ fold-change (LogFC) ≥ 1.5 . A heatmap of these DEGs highlights the differences between LOT and chRCC-*eo* samples identified 175 differentially enriched pathways (Fig. 5C). Of particular interest, mTOR signaling, protein processing in the

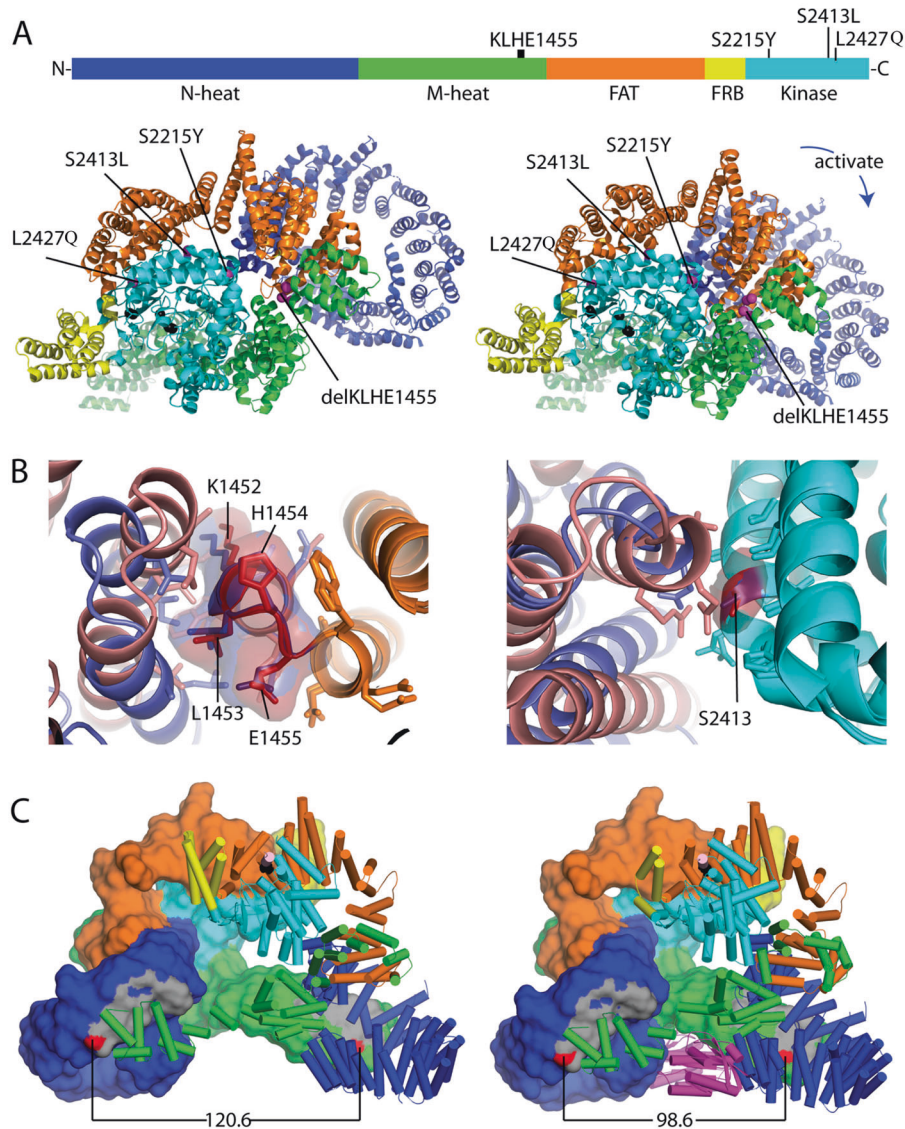


Fig. 2 Schematic mapping of mTOR mutations in LOT samples. **A** Mutation positions in the mTOR protein primary structure as well as tertiary structures of apo mTORC1 (PDB: 6bcx, left) and RHEB-activated mTORC1 (PDB: 6bcu, right) with colored domains. **B** Structure context of less well-characterized mTOR mutations. Left: superimposed wild type mTOR FAT domain hinge region (orange) with an area corresponding to K1452–E1455 (deleted in LOT 6) illustrating differential interactions with neighboring FAT helices in apo (slate) and RHEB activated (salmon) conformations. Residues within 4 Å are in the stick. Right: superimposed kinase C-lobes (cyan) containing the S2413I mutation (LOT 5). The mutation is positioned at the FAT domain interface, which adopts alternate conformations in the active (salmon) and apo (slate) states. Residues within 4 Å are in the stick. **C** mTORC1 dimerization interface is incompatible with mixed dimers. Left: mTOR dimer (domains colored as above) from an apo mTORC1 structure (PDB: 6BCX) with one chain in surface rendering and the second chain in cartoon mode. The dimer interface (gray) is formed by the interaction of N-heat (dark blue) and M-heat domains (green), with the distance between two residues in the dimer interface (N612 and R1161, red) indicated below. Right: RHEB (magenta)-activated mTOR dimer with closer interaction surfaces as shown by the distance between N612 and R1161 (red).

endoplasmic reticulum, and MAPK signaling pathways were enriched in the LOT respective to chRCC-*eo*. Overall, these findings suggest that LOTs have a unique gene expression signature that sets them apart from other tumors.

DISCUSSION

We report comprehensive molecular profiling analyses of a recently described renal tumor entity, LOT, expanding our understanding of this novel disease^{19,21}. Our results show that LOT can present in both syndromic and non-syndromic cases with uniform morphology and IHC features. LOT tumors have converging mutations in mTOR pathway genes and mTORC1 activation. Gene expression analyses

show that LOT has a unique gene expression signature that differs from close morphologic mimics, chRCC-*eo* and RO.

Our results support and expand the morphologic and IHC features previously reported. In 2019, Trpkov et al.,¹⁹ reported 28 distinct LOTs from four institutional archives. All tumors had consistent morphology characterized by tight nests of bland tumor cells with eosinophilic cytoplasm and were devoid of prominent nuclear membrane irregularities. Informatively, LOTs had a unique immunoprofile with CD117 negativity and diffuse CK7 reactivity. These findings were consistently observed in 7 additional cases reported by Guo et al.,²¹ and in the 22 tumors in our series.

These initial studies reported LOTs to be single and devoid of a syndromic association. One patient in our series had multiple

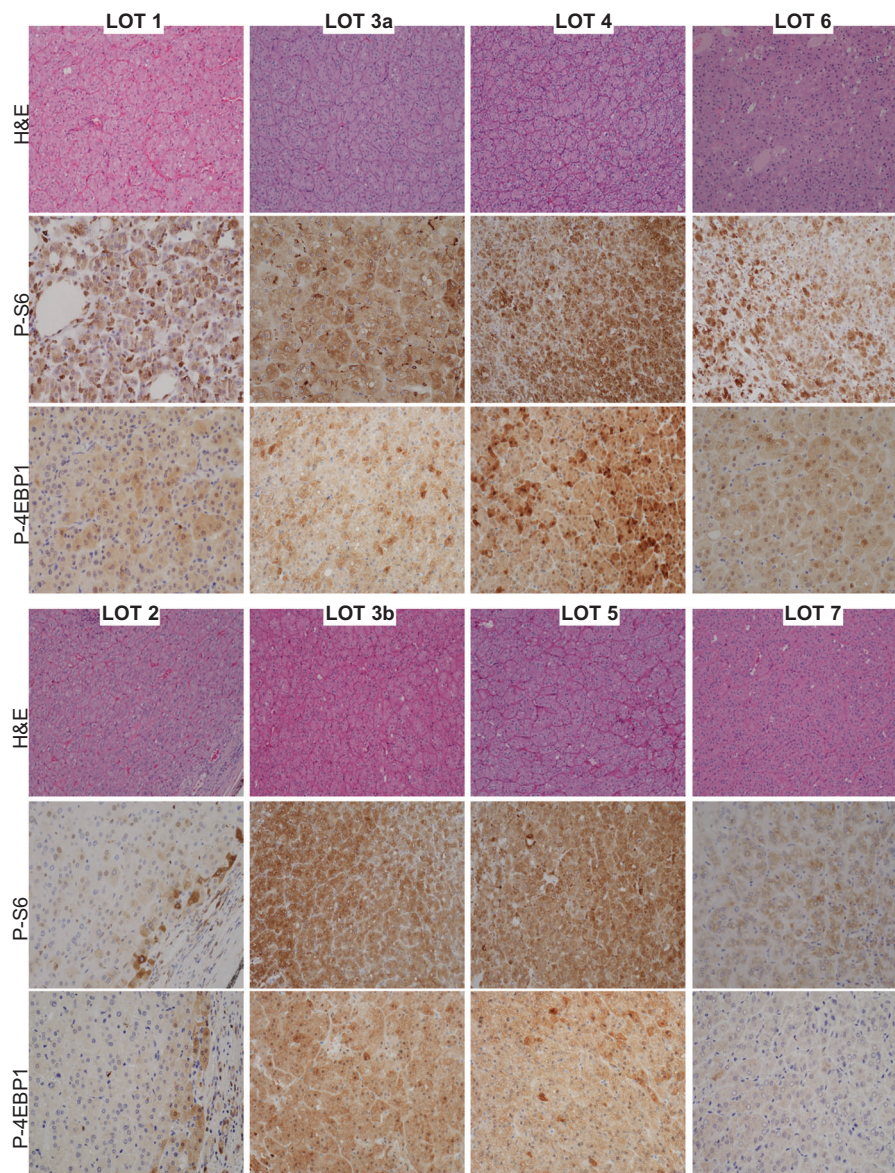


Fig. 3 Evaluation of mTORC1 pathway activation in LOT. Representative H&E, p-S6, and p-4EBP1 immunohistochemical expression in LOTs (at $\times 200$ original magnification). The percentage of tumor cells expressing cytoplasmic phospho-S6 and the intensity of expression is tabulated in the Table 2.

bilateral LOTs and had a likely pathogenic germline *TSC1* mutation. TSC syndrome can have variable penetrance and a significant percent of cases have de novo mutations with no known family history. Individuals may have a mild phenotype, particularly when the *TSC1* gene is implicated⁵⁴. However, it is quite likely that our LOT 3 patient had TSC as the same *TSC1* germline mutation has been reported in a 3-generation family with mild clinical TSC features⁵⁵. All tumors seen in this patient were indistinguishable morphologically and by IHC from other LOTs in our series. A recent study similarly reported multifocal LOTs in TSC and in end-stage renal disease (ESRD)²². None of our patients had ESRD. Similarly, previous studies of kidneys in TSC patients include cases that morphologically resemble LOT histologically and by IHC (CD117 $-$ /CK7 $+$)^{4,5}. These findings support that LOT can occur in both the sporadic and syndromic contexts. Although metastases have not been reported to date in LOT, as illustrated by the benefits seen in our LOT 3 patient, rapalogs may be considered for the management of multiple syndromic LOTs. This is further supported by the observation that

at least in some contexts, mTOR pathway mutations are associated with rapalog responsiveness^{56,57}.

The classification of renal tumors is largely based on morphologic, and to a lesser extent, molecular features. LOT exhibits distinct but overlapping histologic features with chRCC-eo and RO. Using exome and transcriptome sequencing Joshi et al., identified two main subtypes of RO. Type 1 tumors were diploid and exhibited *CCND1* rearrangement. In contrast, Type 2 tumors were hypodiploid with loss of chromosome 1, X/Y, and/or 14 and 21⁴¹. Type 2 tumors could progress to chRCC-eo⁴¹. Our prior work shows that most chRCC-eo are similar to RO, do not have classic chromosomal abnormalities of chRCC, and are often diploid²³. In the TCGA dataset, 10/19 chRCC-eo showed the characteristic chRCC copy number pattern with loss of one copy of entire chromosomes for most chromosomes including 1, 2, 6, 10, 13, 17. In a Swiss cohort, chromosomal losses were observed in 27% of chRCC-eo⁵⁸. Our data and those from others⁵⁹ suggest that LOT, like RO and chRCC-eo, are largely diploid and lack the recurrent chromosomal abnormalities of classic chRCC. It is tempting to

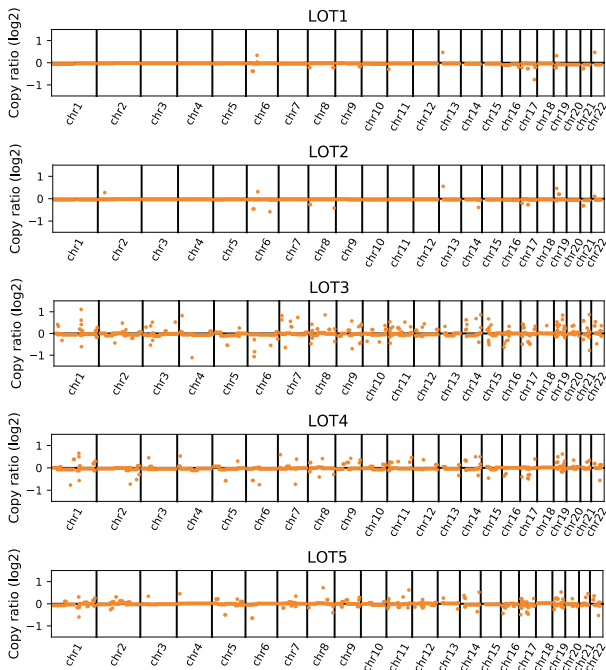


Fig. 4 Copy number analysis in LOT. Whole-genome profiles of \log_2 copy ratio by CNVkit on WES in LOTs. Average \log_2 copy ratio estimations are marked in orange.

speculate a stepwise progression from RO (at least a subset) to chRCC-eo to classic chRCC especially given the link to chromosome 1 loss, which may be a driver event. How LOTs relate to this progression is currently unclear.

Our gene expression analyses show that LOTs have a unique expression profile that distinguishes these tumors from RO and chRCC (both classic and eosinophilic variants). These changes in gene expression likely contribute to differential protein expression (CK7, CD117). Other markers include FOXI1, which is expressed in chRCC-eo and not in LOT⁶⁰. Both CD117 and FOXI1 are expressed in renal intercalated cells of distal tubules, suggesting perhaps that these cells give rise to chRCC-eo but not LOT. In fact, differences in the expression of FOXI1 mRNA in TCGA-pan RCC allowed Tong et al.,⁶⁰ to identify 5 outlier cases (four of which are the same we found to resemble LOT morphologically and one additional TCGA-MH-A857 from KIRP) which they reclassified as “eosinophilic chromophobe-like renal tumors”. Similarly, Skala et al.,⁶¹ found 2 out of their 10 institutional chRCC-eo to have low or absent FOXI1 expression. The morphology of these 2 tumors matches LOT and they were reported to have *MTOR* mutations, were diploid, and lacked chromosome 1 loss (Supplementary Fig. 7A, B). Overall, these data show that LOT are characterized by a distinct gene expression signature and outline the potential of low FOXI1 expression as a diagnostic biomarker.

Our study illustrates that LOT has converging mutations in genes involved in the mTORC1 pathway (*MTOR*, *TSC1*, and *RHEB*). Interestingly, using target gene sequencing, Tjota et al., recently described a spectrum of renal tumors with pathogenic mutations in *TSC1/TSC2/MTOR*^{59,62}. A subset of these tumors (group 2) was CK7+ and had absent to weak (1+) CD117 expression and could represent LOT. Though it may be tempting to classify LOT as “TSC/mTOR-associated renal neoplasms”⁶², these represent a heterogeneous group of tumors based on morphology and IHC. Somatic alterations in mTOR pathway genes have been described in several RCC^{23,52,61–65}. We first reported the identification of mTORC1 pathway gene mutations in ccRCC in 2011, when we found mutations in *TSC1*⁶⁶. Subsequently, mTORC1 pathway gene mutations were reported in chRCC by us and others^{23,52,59,61}.

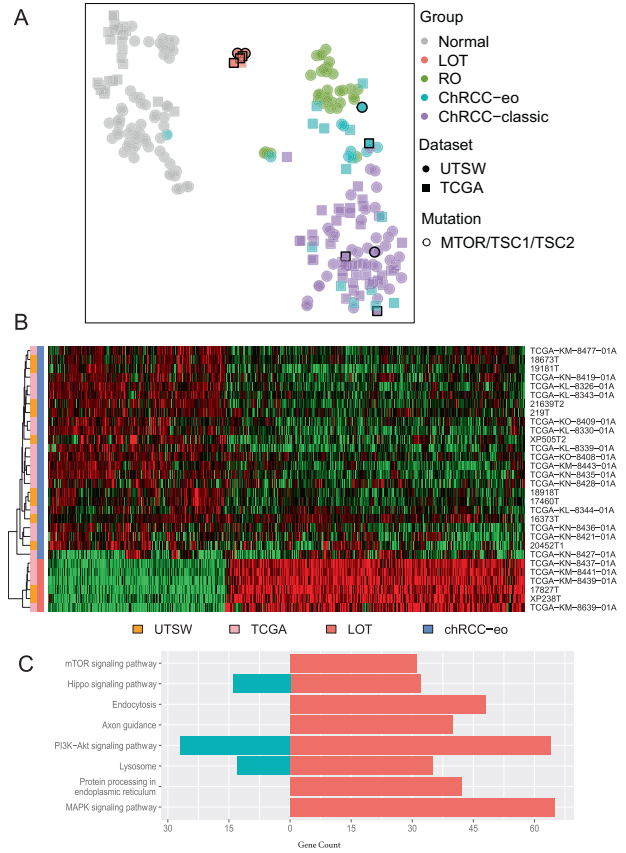


Fig. 5 RNA-seq-based clustering of LOT, RO, and chRCC.

A t-distributed stochastic neighbor embedding (t-SNE) plot of filtered whole transcriptomic data from pooled UTSW and TCGA cohorts showing clustering of LOT samples away from classic chRCC, chRCC-eo, and RO, including chRCC with mTORC1 pathway gene mutations (highlighted with black borders). **B** Heatmap of 1674 most differentially expressed genes distinguishing LOT from chRCC-eo. **C** Select enriched pathways between LOT and chRCC-eo by KEGG analysis of DEGs with over-representation p -value ≤ 0.05 . Up (red) and down (cyan) regulated gene counts are shown.

mTORC1 pathway mutations have also been reported in eosinophilic tumors including EVT and ESC RCC². Thus, mTORC1 pathway mutations alone are not a sufficiently distinguishing feature.

In our cohort, all cases exhibited activation of mTORC1. mTOR is found in two complexes, mTORC1 and mTORC2. Our data suggest that mTORC1 may, in particular, be affected. This idea is supported by the finding of mTORC1 activation (of which p-S6 and p-4EBP1 are specific markers), as well as by mutations in *TSC1* and *RHEB* that specifically regulate mTORC1. The TSC complex is a heterotrimer that includes *TSC1* and *TSC2* as well as *TBC1D7* and acts as a GTPase activating protein (GAP) for the small GTPase *RHEB*⁶⁷. TSC complex inactivation leads to constitutive activation of *RHEB*. In its GTP-bound form, *RHEB* binds and activates mTORC1. mTORC1 plays a central role in coordinating cell growth and metabolism by taking cues from its environments such as the availability of nutrients and growth factors⁶⁷. For a cell to divide, it needs to promote anabolism and increase its mass. mTORC1 is a downstream mediator of several growth factors and mitogen-dependent signaling pathways that converge in the regulation of the TSC complex. Our data suggest that mTORC1 activation is a typical feature of LOT.

In our LOT cases, the levels of mTORC1 activation varied. Interestingly, we noted a correlation between LOT cases with

MTOR gene mutations specifically and lower mTORC1 activation. A potential explanation for this finding is that *MTOR* mutations were heterozygous and the wild-type allele appeared to be preserved. The significance of a preserved wild-type protein may be heightened by the fact that mTORC1 complexes are homodimers. This consideration is particularly interesting by comparison to EVT^{14,17} where *MTOR* activating mutations are typically accompanied by loss of chromosome 1 (and the second copy of *MTOR*). This may contribute to explain the higher grade appearance of EVT compared to LOT. One possibility is that LOT may evolve to EVT upon loss of chromosome 1 (and the remaining *MTOR* wild-type allele). Thus, mTORC1 may serve as a rheostat in LOT, EVT, as well as other tumors with driver mTORC1 pathway alterations and morphologic overlap such as ESC-RCC. Provocatively, and as shown in Supplementary Fig. 2C–F, LOT 3 and LOT 4 showed a focal distinct area that morphologically resembled EVT/chRCC-*eo* with stronger p-S6 expression (data not shown). Furthermore, mTORC1 pathway mutations appear to be associated with worse clinical outcomes in chRCC⁶⁸. While this makes sense conceptually, most tumors described to date (and our own observations) do not show morphologic subclones suggestive of progression. As alluded to above, it is also possible that they involve different cells of origin. Thus, the extent to which these tumors are related remains to be fully determined.

In summary, our study provides a comprehensive molecular, and histopathologic analysis of low-grade oncocytic tumors, a recently described renal cell neoplasm. We show that they exhibit a unique gene expression signature that distinguishes them from morphologically-related tumors, as well as consistent mTORC1 pathway mutations and broaden the clinical presentation to include syndromic patients. Our data support LOT as a unique and distinct entity of indolent clinical behavior.

DATA AVAILABILITY

The datasets used and analyzed during the current study are available from the corresponding author on reasonable request.

REFERENCES

- Trpkov, K., et al. New developments in existing WHO entities and evolving molecular concepts: the genitourinary pathology society (GUPS) update on renal neoplasia. *Mod Pathol* <https://doi.org/10.1038/s41379-021-00779-w> (2021).
- Trpkov, K. et al. Novel, emerging and provisional renal entities: the genitourinary pathology society (GUPS) update on renal neoplasia. *Mod Pathol* **34**, 1167–1184 (2021).
- Williamson, S. R. et al. Diagnostic criteria for oncocytic renal neoplasms: a survey of urologic pathologists. *Hum Pathol* **63**, 149–156 (2017).
- Guo, J. et al. Tuberous sclerosis-associated renal cell carcinoma: a clinicopathologic study of 57 separate carcinomas in 18 patients. *Am J Surg Pathol* **38**, 1457–1467 (2014).
- Yang, P. et al. Renal cell carcinoma in tuberous sclerosis complex. *Am J Surg Pathol* **38**, 895–909 (2014).
- Pavlovich, C. P. et al. Renal tumors in the Birt-Hogg-Dube syndrome. *Am J Surg Pathol* **26**, 1542–1552 (2002).
- McKenney, J. K., Przybycin, C. G., Trpkov, K. & Magi-Galluzzi, C. Eosinophilic solid and cystic renal cell carcinomas have metastatic potential. *Histopathology* **72**, 1066–1067 (2018).
- Trpkov, K. et al. Eosinophilic solid and cystic renal cell carcinoma (ESC RCC): further morphologic and molecular characterization of ESC RCC as a distinct entity. *Am J Surg Pathol* **41**, 1299–1308 (2017).
- Trpkov, K. et al. Eosinophilic, solid, and cystic renal cell carcinoma: clinicopathologic study of 16 unique, sporadic neoplasms occurring in women. *Am J Surg Pathol* **40**, 60–71 (2016).
- Argani, P. MIT family translocation renal cell carcinoma. *Semin Diagn Pathol* **32**, 103–113 (2015).
- Srigley, J. R. et al. The international society of urological pathology (ISUP) Vancouver classification of renal neoplasia. *Am J Surg Pathol* **37**, 1469–1489 (2013).
- Gill, A. J. et al. Succinate dehydrogenase (SDH)-deficient renal carcinoma: a morphologically distinct entity: a clinicopathologic series of 36 tumors from 27 patients. *Am J Surg Pathol* **38**, 1588–1602 (2014).
- Smith, S. C. et al. A distinctive, low-grade oncocytic fumarate hydratase-deficient renal cell carcinoma, morphologically reminiscent of succinate dehydrogenase-deficient renal cell carcinoma. *Histopathology* **71**, 42–52 (2017).
- Trpkov, K. et al. High-grade oncocytic tumour (HOT) of kidney in a patient with tuberous sclerosis complex. *Histopathology* **75**, 440–442 (2019).
- He, H. et al. "High-grade oncocytic renal tumor": morphologic, immunohistochemical, and molecular genetic study of 14 cases. *Virchows Arch* **473**, 725–738 (2018).
- Chen, Y. B. et al. Somatic mutations of TSC2 or MTOR characterize a morphologically distinct subset of sporadic renal cell carcinoma with eosinophilic and vacuolated cytoplasm. *Am J Surg Pathol* **43**, 121–131 (2019).
- Kapur, P., et al. Eosinophilic vacuolated tumor of the kidney: a review of evolving concepts in this novel subtype with additional insights from a case with MTOR mutation and concomitant chromosome 1 loss. *Adv Anat Pathol* <https://doi.org/10.1097/PAP.0000000000000299> (2021).
- Chen, Y. B. et al. Molecular analysis of aggressive renal cell carcinoma with unclassified histology reveals distinct subsets. *Nat Commun* **7**, 13131 (2016).
- Trpkov, K. et al. Low-grade oncocytic tumour of kidney (CD117-negative, cytokeratin 7-positive): a distinct entity? *Histopathology* **75**, 174–184 (2019).
- Siadat, F. & Trpkov, K. ESC, ALK, HOT and LOT: three letter acronyms of emerging renal entities knocking on the door of the WHO classification. *Cancers* **12** (2020).
- Guo, Q. et al. Characterization of a distinct low-grade oncocytic renal tumor (CD117-negative and cytokeratin 7-positive) based on a tertiary oncology center experience: the new evidence from China. *Virchows Arch* <https://doi.org/10.1007/s00428-020-02927-0> (2020).
- Kravtsov, O., et al. Low-grade oncocytic tumor of kidney (CK7-positive, cd117-negative): incidence in a single institutional experience with clinicopathological and molecular characteristics. *Hum Pathol* <https://doi.org/10.1016/j.humpath.2021.04.013> (2021).
- Durinck, S. et al. Spectrum of diverse genomic alterations define non-clear cell renal carcinoma subtypes. *Nat Genet* **47**, 13–21 (2015).
- Trpkov, K. & Hes, O. New and emerging renal entities: a perspective post-WHO 2016 classification. *Histopathology* **74**, 31–59 (2019).
- Pena-Llopis, S. & Brugarolas, J. Simultaneous isolation of high-quality DNA, RNA, miRNA and proteins from tissues for genomic applications. *Nat Protoc* **8**, 2240–2255 (2013).
- Li, H. & Durbin, R. Fast and accurate short read alignment with Burrows–Wheeler transform. *Bioinformatics* **25**, 1754–1760 (2009).
- DePristo, M. A. et al. A framework for variation discovery and genotyping using next-generation DNA sequencing data. *Nat Genet* **43**, 491–498 (2011).
- McKenna, A. et al. The genome analysis toolkit: a MapReduce framework for analyzing next-generation DNA sequencing data. *Genome Res* **20**, 1297–1303 (2010).
- Van der Auwera, G. A., et al. From FastQ data to high confidence variant calls: the genome analysis toolkit best practices pipeline. *Curr Protoc Bioinform* **43**, 11 10 11–33 (2013).
- Cibulskis, K. et al. Sensitive detection of somatic point mutations in impure and heterogeneous cancer samples. *Nat Biotechnol* **31**, 213–219 (2013).
- Koboldt, D. C. et al. VarScan 2: somatic mutation and copy number alteration discovery in cancer by exome sequencing. *Genome Res* **22**, 568–576 (2012).
- Hansen, N. F., Gartner, J. J., Mei, L., Samuels, Y. & Mullikin, J. C. Shimmer: detection of genetic alterations in tumors using next-generation sequence data. *Bioinformatics* **29**, 1498–1503 (2013).
- Chiang, C. et al. SpeedSeq: ultra-fast personal genome analysis and interpretation. *Nat Methods* **12**, 966–968 (2015).
- Saunders, C. T. et al. Strelka: accurate somatic small-variant calling from sequenced tumor-normal sample pairs. *Bioinformatics* **28**, 1811–1817 (2012).
- Wang, K., Li, M. & Hakonarson, H. ANNOVAR: functional annotation of genetic variants from high-throughput sequencing data. *Nucleic Acids Res* **38**, e164 (2010).
- Wang, T. et al. Probability of phenotypically detectable protein damage by ENU-induced mutations in the mutagenetix database. *Nat Commun* **9**, 441 (2018).
- Talevich, E., Shain, A. H., Botton, T. & Bastian, B. C. CNVkit: genome-wide copy number detection and visualization from targeted DNA sequencing. *PLoS Comput Biol* **12**, e1004873 (2016).
- Turajlic, S. et al. Deterministic evolutionary trajectories influence primary tumor growth: TRACERx renal. *Cell* **173**, 595–610 e511 (2018).
- Dobin, A. et al. STAR: ultrafast universal RNA-seq aligner. *Bioinformatics* **29**, 15–21 (2013).
- Liao, Y., Smyth, G. K. & Shi, W. featureCounts: an efficient general purpose program for assigning sequence reads to genomic features. *Bioinformatics* **30**, 923–930 (2014).
- Joshi, S. et al. The genomic landscape of renal oncocytoma identifies a metabolic barrier to tumorigenesis. *Cell Rep.* **13**, 1895–1908 (2015).

42. Robinson, M. D., McCarthy, D. J. & Smyth, G. K. edgeR: a bioconductor package for differential expression analysis of digital gene expression data. *Bioinformatics* **26**, 139–140 (2010).
43. Robinson, M. D. & Oshlack, A. A scaling normalization method for differential expression analysis of RNA-seq data. *Genome Biol* **11**, R25 (2010).
44. Johnson, W. E., Li, C. & Rabinovic, A. Adjusting batch effects in microarray expression data using empirical Bayes methods. *Biostatistics* **8**, 118–127 (2007).
45. Zhao, S. et al. A brain somatic RHEB doublet mutation causes focal cortical dysplasia type II. *Exp Mol Med* **51**, 84 (2019).
46. Xu, J. et al. Mechanistically distinct cancer-associated mTOR activation clusters predict sensitivity to rapamycin. *J Clin Invest* **126**, 3526–3540 (2016).
47. Lim, J. S. et al. Brain somatic mutations in MTOR cause focal cortical dysplasia type II leading to intractable epilepsy. *Nat Med* **21**, 395–400 (2015).
48. Yang, H. et al. Mechanisms of mTORC1 activation by RHEB and inhibition by PRAS40. *Nature* **552**, 368–373 (2017).
49. Wagle, N. et al. Activating mTOR mutations in a patient with an extraordinary response on a phase I trial of everolimus and pazopanib. *Cancer Discov* **4**, 546–553 (2014).
50. Ghosh, A. P. et al. Point mutations of the mTOR-RHEB pathway in renal cell carcinoma. *Oncotarget* **6**, 17895–17910 (2015).
51. Yang, H. et al. mTOR kinase structure, mechanism and regulation. *Nature* **497**, 217–223 (2013).
52. Davis, C. F. et al. The somatic genomic landscape of chromophobe renal cell carcinoma. *Cancer Cell* **26**, 319–330 (2014).
53. Ohne, Y. et al. Isolation of hyperactive mutants of mammalian target of rapamycin. *J Biol Chem* **283**, 31861–31870 (2008).
54. Au, K. S. et al. Genotype/phenotype correlation in 325 individuals referred for a diagnosis of tuberous sclerosis complex in the United States. *Genet Med* **9**, 88–100 (2007).
55. Streff, H. et al. TSC1 variant associated with mild or absent clinical features of tuberous sclerosis complex in a three-generation family. *Pediatr Neurol* **110**, 89–91 (2020).
56. Wolff, N. et al. Sirolimus and temsirolimus for epithelioid angiomyolipoma. *J Clin Oncol* **28**, e65–e68 (2010).
57. Maroto, P. et al. Biallelic TSC2 mutations in a patient with chromophobe renal cell carcinoma showing extraordinary response to temsirolimus. *J Natl Compr Canc Netw* **16**, 352–358 (2018).
58. Ohashi, R., et al. Classic chromophobe renal cell carcinoma incur a larger number of chromosomal losses than seen in the eosinophilic subtype. *Cancers* **11** (2019).
59. Tjota, M. Y., Wanjari, P., Segal, J. & Antic, T. TSC/MTOR mutated eosinophilic renal tumors are a distinct entity that are CK7+/CK20-/vimentin-: a validation study. *Hum Pathol* <https://doi.org/10.1016/j.humpath.2020.12.006> (2020).
60. Tong, K. & Hu, Z. FOXI1 expression in chromophobe renal cell carcinoma and renal oncocytoma: a study of The Cancer Genome Atlas transcriptome-based outlier mining and immunohistochemistry. *Virchows Arch* <https://doi.org/10.1007/s00428-020-02900-x> (2020).
61. Skala, S. L. et al. Next-generation RNA sequencing-based biomarker characterization of chromophobe renal cell carcinoma and related oncocytic neoplasms. *Eur Urol* **78**, 63–74 (2020).
62. Tjota, M. et al. Eosinophilic renal cell tumors with a TSC and MTOR gene mutations are morphologically and immunohistochemically heterogeneous: clinicopathologic and molecular study. *Am J Surg Pathol* **44**, 943–954 (2020).
63. Ricketts, C. J. et al. The Cancer Genome Atlas comprehensive molecular characterization of renal cell carcinoma. *Cell Rep* **23**, 313–326 e315 (2018).
64. Cancer Genome Atlas Research, N. Comprehensive molecular characterization of clear cell renal cell carcinoma. *Nature* **499**, 43–49 (2013).
65. Linehan, W. M. & Ricketts, C. J. The Cancer Genome Atlas of renal cell carcinoma: findings and clinical implications. *Nat Rev Urol* **16**, 539–552 (2019).
66. Kucejova, B. et al. Interplay between pVHL and mTORC1 pathways in clear-cell renal cell carcinoma. *Mol Cancer Res* **9**, 1255–1265 (2011).
67. Saxton, R. A. & Sabatini, D. M. mTOR signaling in growth, metabolism, and disease. *Cell* **168**, 960–976 (2017).
68. Roldan-Romero, J. M. et al. Molecular characterization of chromophobe renal cell carcinoma reveals mTOR pathway alterations in patients with poor outcome. *Mod Pathol* **33**, 2580–2590 (2020).

ACKNOWLEDGEMENTS

We acknowledge the patients whose samples provided the foundation for this study and are grateful to the Kidney Cancer Program and the Clinical Data Warehouse teams for their support and assistance.

AUTHOR CONTRIBUTIONS

P.K., H.Z., and J.B. designed and performed the research, analyzed and interpreted data, and wrote the paper. M.G. performed sanger sequencing. P.K. and S.C. performed the pathological review of the cases. H.Z. performed the molecular analysis. M.M., S.B., Q.Z., L.X., J.B., and P.K. helped interpret molecular data. J.M. and D.C. performed IHCs. D.R. and V.M. provided technical support. L.K. provided interpretation of crystal structure. I.P. provided radiologic images and their interpretation. P.K. assembled the clinical data. All authors read and approved the final paper.

FUNDING

This work was supported by the NIH-sponsored Kidney Cancer SPORE grant (P50CA196516) and endowment from Jan and Bob Pickens Distinguished Professorship in Medical Science and Brock Fund for Medical Science Chair in Pathology.

COMPETING INTERESTS

The authors declare no competing interests.

ETHICS

The study was conducted with approval by the UT Southwestern Medical Center (UTSW) Institutional Review Board (IRB) and according to the Health Insurance Portability and Accountability Act (HIPAA) guidelines (STU 022013-052).

ADDITIONAL INFORMATION

Supplementary information The online version contains supplementary material available at <https://doi.org/10.1038/s41379-021-00896-6>.

Correspondence and requests for materials should be addressed to Payal Kapur or James Brugarolas.

Reprints and permission information is available at <http://www.nature.com/reprints>

Publisher's note Springer Nature remains neutral with regard to jurisdictional claims in published maps and institutional affiliations.